RSC Advances

PAPER

View Article Online
View Journal | View Issue

Cite this: *RSC Adv.*, 2014, **4**, 60371

Ionic liquid electrodeposition of 3D germanium–acetylene black–Ni foam nanocomposite electrodes for lithium-ion batteries†

Jian Hao,[ab] Xiaoxu Liu,[a] Na Li,[a] Xusong Liu,[a] Xiaoxuan Ma,[a] Yi Zhang,[c] Yao Li*[c] and Jiupeng Zhao*[ab]

Received 22nd September 2014
Accepted 4th November 2014

DOI: 10.1039/c4ra10931g

www.rsc.org/advances

A simple process involving the electrophoretic deposition of acetylene black onto Ni foam and the ionic liquid electrodeposition of Ge has been used to synthesize a 3D Ge–acetylene black–Ni foam electrode material at room temperature. Electrochemical measurements demonstrate that when applied in a lithium ion battery, this material exhibits a high capacity of up to 924 mA h g^{-1} after 100 cycles at 0.1 C and a high rate capability at 1 C and 5 C rates of 1210 and 524 mA h g^{-1}, respectively. This high electrochemical performance is the result of the 3D acetylene black network enhancing electron migration, while also providing sufficient elasticity to buffer the volume expansion of the Ge nanoparticles.

Introduction

Lithium-ion batteries (LIBs) are currently used in a range of portable electronic devices such as phones, personal computers, digital cameras, *etc.*, which has led to them being considered for use in powering hybrid and zero emission electric vehicles.[1,2] However, in order to meet the requirements for such use, there is a need to achieve a much higher energy and power density.[3,4] At present, graphite is the most commonly used material for the negative electrode in commercial LIBs, but its relatively low theoretical capacity of 372 mA h g^{-1} greatly limits its performance.[5] Silicon, germanium and their compounds are important semiconductors have large potential application in the fields of electronics and photonics. Especially, for lithium ion battery, Si and Ge as lithium-ion battery cathode materials, for their high specific capacity (Si 4200 mA h g^{-1},[6] Ge 1600 mA h g^{-1} [7]), respectively, forming the $Li_{22}M_5$ alloy. But alloy anodes undergo significant volume expansion and contraction during Li insertion/extraction (up to 400% in the case of Si). This volume change can result in pulverization of the initial morphology and a subsequent loss of electrical contact between active materials and the electrode framework.[8] To alleviate this problem, various forms of Si electrode materials have been studied, including nanowires,[9] nanotubes,[10] thin films,[11] nanoparticles[12] and 3D porous particles.[13] However, the slow kinetics of lithium transport in Si results in a poor rate capability, which limits their suitability for use in high-rate LIBs. The lower capacity of Ge has seen it receive much less attention than Si, yet the diffusivity of Li in Ge at room temperature is about 400 times greater than that of Si. Furthermore, the smaller band gap of Ge (0.6 eV) results in an electrical conductivity that is in the order of 10^4 greater than Si, thus making Ge an attractive electrode material for high-charging-rate LIBs.[14] The downside to Ge-based materials is that although there are a number of methods by which they can be produced such as CVD,[15] electron beam evaporation,[16] magnetron sputtering,[17] the solvothermal method,[18] *etc.*, these are generally either too complicated or require reaction temperatures that are too high to be of commercial interest. There is therefore a very real need for a low-temperature method of synthesizing Ge electrodes that is both efficient and environmentally sound.

Electrodeposition represents a low-cost and viable technique for the synthesis of metals and alloys from aqueous solution, yet despite being the subject of considerable research, it is limited by the fact hydrogen will evolve before any Ge- or Si-based semiconductor can be formed. However, the wider electrochemical window offered by ionic liquids[19] presents a possible solution to this problem, and indeed the authors have already extensively studied the electrodeposition of Ge from such liquids.[20–22] Despite this, the practical use of Ge as an electrode material is still hindered by its dramatic volume change (300%) during Li insertion/extraction.[23] To overcome this problem,

[a]*School of Chemical Engineering and Technology, Harbin Institute of Technology, 150001, Harbin, China. E-mail: jiupengzhao@126.com; Fax: +86 451 86402345; Tel: +86 451 86402345*

[b]*State Key Laboratory of Advanced Welding and Joining, Harbin Institute of Technology, Harbin 150001, China*

[c]*Center for Composite Material, Harbin Institute of Technology, Harbin, China. E-mail: liyao@hit.edu.cn; Fax: +86 451 86402345; Tel: +86 451 86402345*

† Electronic supplementary information (ESI) available: EDS spectra of 3D Ge–acetylene black–Ni foam electrode, XRD pattern of acetylene black and the Ge acetylene black, BET surface area of acetylene black and the Ge acetylene black and SEM image of 3D Ge–acetylene black–Ni foam electrode after 100 cycles at 0.1 C. See DOI: 10.1039/c4ra10931g

various forms of Ge electrode materials have been developed such as nanoparticles,[24] nanowires,[25,26] nanotubes[27] and carbon-coated Ge.[28–30] Of these, it is the latter that seems the most attractive for improving cycling performance, as the moderate Li ion and electron transport kinetics of carbon not only help cushion volume expansion, but also offers fast electron transfer and an enhanced energy density. On the other hand, the reduced size of nanoscale Ge particles can help mitigate the physical strain produced by Li uptake/release, effectively accommodating any volume change and preventing pulverization. Nanoscale structures have also shown quite promising capacities and cycling stability, with the Ge@C/RGO nanocomposite produced by Li-Jun Wan *et al.* retaining a reversible capacity of ~940 mA h g^{-1} after 50 cycles at a current density of 50 mA g^{-1}. Such results can be attributed to the electrically conductive and elastic RGO network, as well as the carbon shells and small size of the Ge NPs.[31] Yu's group has also succeeded in synthesizing carbon-encapsulated Ge and GeOx nanowires by pyrolysis, which exhibited excellent Li storage properties of 1200 and 1000 mA h g^{-1} at 0.2 C for Ge/C and GeOx/C, respectively.[32]

In addition to the electrode material, the current collector used also plays an extremely important role in determining the performance of a LIB. Copper foil is typically used as the current collector in LIBs,[33] onto which the electrode is fabricated as a thin film by mixing active materials with polymer binders and conductive additives. However, the presence of these inert binders and additives greatly reduces the Li ion migration rate of the electrode, resulting in a poor rate capability and significant decrease in energy density. Hence, three-dimensional (3D) electrodes with a nanostructured architecture, which does not rely on polymer binders or conductive additives, have attracted a great deal of attention as a means of achieving both a fast electron transfer and an enhanced energy density.

In this study, a 3D Ge–acetylene black–Ni foam electrode was constructed based on the following ideas:

(1) Ni foams have a 3D structure that has the ability to incorporate active materials into the current collector, rather than merely depositing them on the surface.

(2) Acetylene black provides a highly conductive and flexible matrix, which not only provides good electrical contact over its whole surface, but also accommodates the huge volume change of Ge particles during cycling.

(3) Ionic liquid electrodeposition allows for fabrication of a 3D structure without the need for a current collector or binder.

In this paper, we first report a feasible method to construct a novel 3D Ge–acetylene black–Ni foam nanoarchitecture by ionic liquid electrodeposition. A typical procedure for the synthesis of the 3D Ge–acetylene-black–Ni foam anode is shown in Fig. 1. In this, a Ni foam substrate is first coated with acetylene-black by electrophoresis at room temperature. Next, Ge particles are directly electrodeposited onto this 3D acetylene-black–Ni foam network using new-generation ionic liquids. The resulting uniform film of 3D Ge–acetylene black–Ni foam exhibits sufficient adhesion to substrates to allow it to be used directly as an electrode without further treatment.

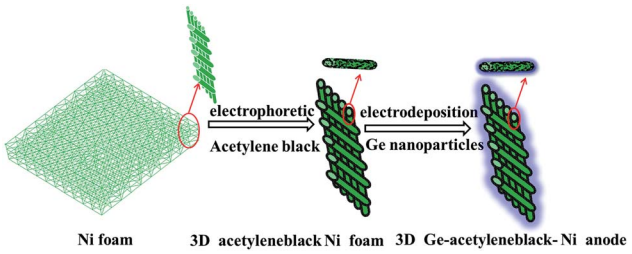

Fig. 1 Schematic illustration showing the synthesis of a 3D Ge–acetylene black–Ni foam electrode.

Experimental

To produce the carbon film on the Ni foam, 20 mg of acetylene black and 4 mg of $Ni(NO_3)_2 \cdot 5H_2O$ were added to 50 mL of isopropyl alcohol and dispersed using a bath-type ultrasonicator for several hours. Cathodic electrophoretic deposition of this suspension was then performed at a constant voltage of 100 V for 2 min with the Ni foam acting as the cathode and Cu foil providing the anode. The resulting films were dried at 80 °C in a vacuum oven for 4 h. For the electrodeposition of the Ge particles, $GeCl_4$ (99.998%) was purchased from Alfa Aesar and used without any further purification. The ionic liquid used was 1-ethyl-3-methylimidazolium bis (trifluoromethylsulfonyl) amide ($EmimTf_2N$, 99%), which was purchased from IOLITEC (Germany) and dried under vacuum at 100 °C for 24 hours to ensure a water content of typically less than 2 ppm.

All electrochemical experiments were performed in an argon-filled glove box with a water and oxygen content of less than 2 ppm (Vigor glove box, Suzhou, China). The electrochemical cell itself was constructed of Teflon and clamped using a Viton O-ring onto a pre-cleaned (in HCl) Ni foam working electrode to provide a total area of about 1.5 cm^2. An Ag wire and Pt ring were used as quasi-reference and counter electrodes, respectively, and a copper wire in contact with the Ni foam was used to provide an electrical connection to the potentiostat. The electrolyte was a 0.1 mol L^{-1} $GeCl_4$ $EmimTf_2N$ solution. Electrochemical measurements were performed using a VersaStat 2273 (Princeton Applied Research) potentiostat/galvanostat controlled by Powersuite software. Cyclic voltammetry (CV) measurements were performed at a scan rate of 10 mV s^{-1} across a range of −2.8 to 1 V relative to the quasi reference electrode at 25 °C. Following experimentation, ultra-pure isopropanol purchased from Alfa Aesar was used to remove any residual ionic liquid.

The morphology of the electrodes was then observed using a Hitachi S-4800 scanning electron microscope operating at 20 kV.

For electrochemical testing, coin-type half-cells (CR2016) were fabricated in an Ar-filled glove box from a 3D Ge–acetylene black–Ni foam electrode, Li metal, a microporous polyethylene separator, and an electrolyte consisting of 1 M $LiPF_6$ in a 1 : 1 : 1 vol% ethylene carbonate (EC)/ethyl methyl carbonate (EMC)/dimethyl carbonate (DMC) solution. The performance of these cells was assessed for 100 cycles between 0.01 and 2.0 V using a

Neware battery testing system (Shenzhen, China) at a current density of 0.1 C.

Results and discussion

The SEM images in Fig. 2a and b show that the surface of the Ni foam current collector was uniformly covered with a randomly oriented, homogenous growth of acetylene black, producing a suitable 3D framework for the fast transfer of electrons. In Fig. 2c and d, it can be seen that Ge nanoparticles were subsequently deposited onto this acetylene black surface as both individual particles and clusters. These clusters are considered responsible for an increase in the surface roughness, but the similarity in morphology between the Ge nanoparticles and the acetylene black makes it difficult to clearly distinguish between the two. In addition to the Ni in the substrate, the EDS results obtained (ESI, Fig. S1†) confirms a uniform distribution of Ge and C in the 3D anode. The elemental distribution in the 3D anode was analyzed by EDS spectroscopy mapping, which was taken over the region in Fig. 2d. The obtained distributions of C and Ge are shown in Fig. 2e and f, respectively. The two elements show a uniform distribution in the whole composite, indicating Ge nanoparticles has been dispersed on 3D carbon network uniformly. A powder XRD pattern of composite shows the diffraction peaks are corresponding to (111), (220), (311) and (331) planes of the diamond structure of Ge, respectively (JCPDS number 00-004-0545). A broad peak at 20–30° is attributed to the amorphous carbon (ESI, Fig. S2†). The BET results showed the BET surface area was decreased from 93.8674 to 82.7768 $m^2\ g^{-1}$ after electrodeposition (ESI, Table. S1†). The above information implies that the Ge–acetylene-black composite is composed of ultrafine Ge nanoparticles dispersed on 3D carbon–Ni foam network uniformly. This unique structure of tightly linked active Ge nanoparticles combined with an elastic 3D acetylene black–Ni foam network is expected to not only improve cycling performance, but as also the mechanical properties of the electrode.

The discharge/charge capacities of a LIB half-cell containing Ge–acetylene black–Ni foam as an active electrode material were measured and compared against those for a Ge–Ni foam. These are shown in Fig. 3a as a function of cycle number at a rate of 0.1 C between 0.01 and 2.0 V, with a 1 C rate being defined as the theoretical capacity of Ge (1600 mA h g^{-1}). This reveals that the use of acetylene black produces an initial discharge and charge capacities of 1652 and 1237 mA h g^{-1}, respectively, with an initial Coulombic efficiency of 74%. In contrast, the initial discharge and charge capacities of the Ge–Ni foam anode were 1830 and 1369 mA h g^{-1}, respectively, with an initial Coulombic efficiency of 80% (Fig. 3b). This loss of initial irreversible capacity can be mainly ascribed to irreversible Li insertion into the nanocomposite, as well as the formation of a solid electrolyte interface on the surface of the electrode.[29,34] However, even though the composite electrode exhibits a lower capacity in the first cycle, the reversibility of its capacity is significantly improved over the whole of the discharge/charge process. As a result, this electrode demonstrates an extremely high performance, achieving a reversible capacity of 924 mA h g^{-1} after 100 cycles.

The reversible capacity of the electrode is a key parameter in the performance of LIBs, with the cycling performance and Coulombic efficiency of the Ge–acetylene black–Ni foam and Ge–Ni foam up to 100 cycles shown in Fig. 3c and d. It can be

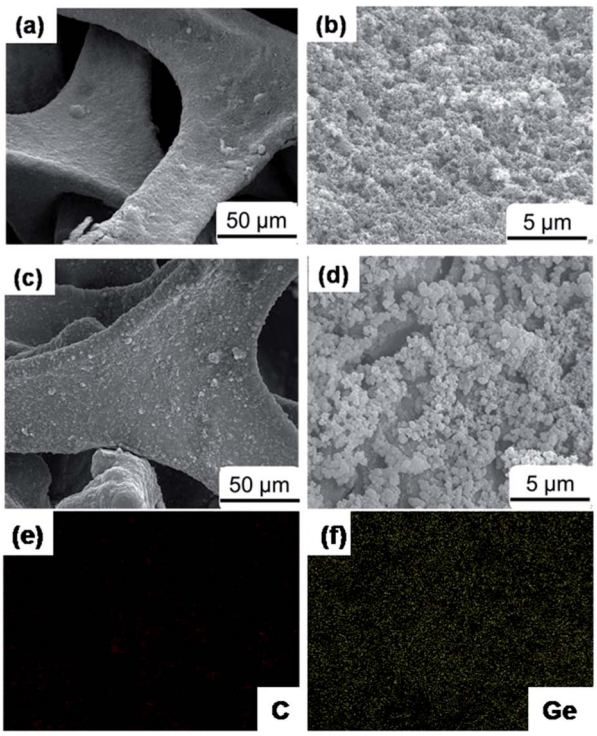

Fig. 2 Typical SEM image (a) and its enlarged images (b) of the 3D acetylene-black–Ni foam networks, (c) and its enlarged images (d) of the 3D germanium–acetylene-black–Ni foam anode materials. (e) and (f) are the corresponding element distributions of image(d).

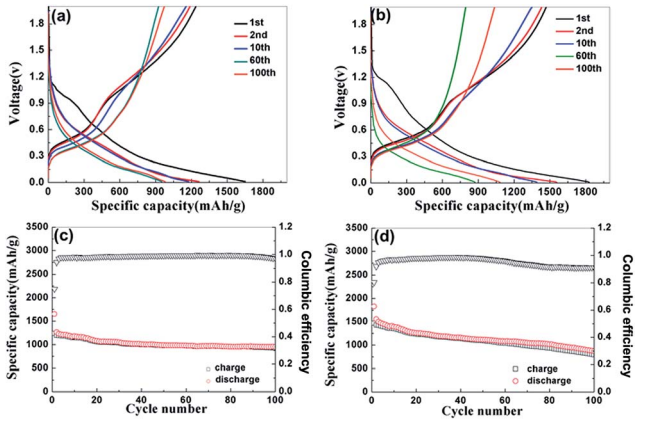

Fig. 3 Charge/discharge curves for a (a) 3D Ge–acetylene black–Ni foam anode and (b) 3D Ge–Ni foam anode at 1st, 2nd, 10th, 60th and 100th cycle, respectively. Cycling performance and coulombic efficiency of (c) 3D Ge–acetylene black–Ni foam anode and (d) 3D Ge–Ni foam anode at a charge/discharge rate of 0.1 C (red: discharge, black: charge).

clearly seen in this that the pure Ge–Ni foam nanofilm exhibits experiences a rapid loss of capacity in the first 20 cycles, with only 48% (871 mA h g^{-1}) being retained after 100 cycles. In contrast, the Ge–acetylene black–Ni foam composite shows great improvement in the cycling performance, with an average columbic efficiency of >98% for up to 100 cycles after the second cycle. This excellent cycling stability indicates that Ge nanoparticles are effectively stabilized during the charge/discharge process.

The rate capabilities of the Ge–acetylene black–Ni foam and Ge–Ni foam nanofilms were tested by sequentially measuring their capacity as the discharge/charge rate was increased from 0.1 to 5.0 C, and then returned to 0.1 C (Fig. 4). We can see from this that as the rate is increased to 2.0 C, there is a small decrease in the discharge capacity of the Ge–acetylene black–Ni foam anode from 1210 to 1002 mA h g^{-1}, while the Ge–Ni foam decreases from 910 to 750 mA h g^{-1}. With further increase to 5.0 C, the discharge capacity decreased to 514 and 309 mA h g^{-1}, respectively. More interesting, however, is the fact that when the rate was returned to 0.1 C, the Ge–acetylene black–Ni foam increased back to 1600 mA h g^{-1}, whereas the Ge–Ni foam increased to just 1260 mA h g^{-1}. Thus, not only does Ge–acetylene black–Ni foam have a much higher rate capability, but this capacity displays excellent stability even when subjected to cycling at higher rates.

The excellent capacity retention and higher rate capability of the Ge–acetylene black–Ni foam composite are attributed to its unique structure, which helps prevent the loss of capacity seen with pure Ge due to its severe volume change during charge/discharge. Specifically, the network structure of the Ni foam provides a much more flexible space for the electrode to expand or self-adjust, while also providing fast electron transfer. Indeed, the 3D remained intact even after 100 cycles (ESI, Fig. S3†). The nanostructure of the active material is also beneficial to the cycling stability, as it reduces the absolute volume change. Moreover, the acetylene black network can potentially provide a powerful elastic buffer, limiting excessive volume expansion of the Ge, as well as providing fast electron transfer and greater energy density. The presence of 3D acetylene black–Ni foam in the nanostructure plays an important role in improving the electrode energy density, which provided fast charge transferring (due to short diffusion length) as well as rapid electrochemical reactions (owing to enlarged surface area).

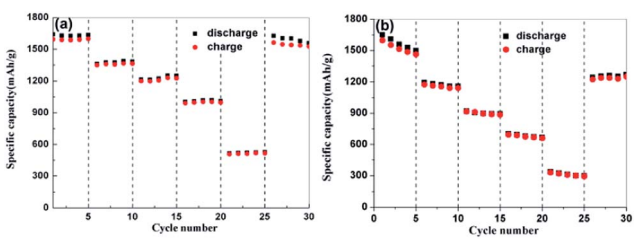

Fig. 4 Rate performance at a 0.1 C, 0.5 C, 1 C, 2 C and 5 C rate of a (a) 3D Ge–acetylene black–Ni foam anode and (b) 3D Ge–Ni foam anode.

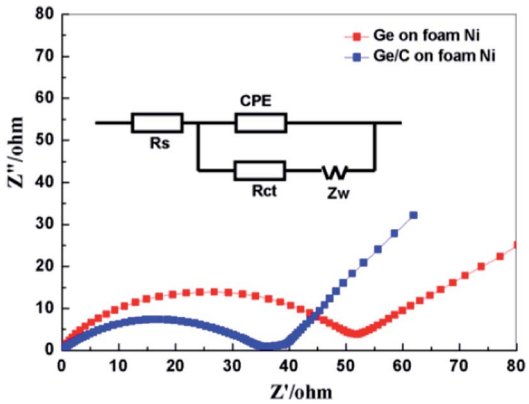

Fig. 5 Impedance spectra for a 3D Ge–acetylene black–Ni foam electrode and 3D Ge–Ni foam electrode after 100 cycles. The inset depicts the equivalent circuit model.

Electrochemical impedance spectroscopy (EIS) measurements of the two nanofilms were conducted using a sine wave of 10 mV amplitude over a frequency range of 100–0.01 Hz. The resulting Nyquist plots (Fig. 5) consist of a depressed semicircle in the high to mid frequency region and an inclined line in the low-frequency region. Both plots can be analyzed using the same Randles equivalent circuit (inset of Fig. 5), in which CPE represents the constant phase-angle element of the double-layer capacitance. The intercept on the *Z*-real axis in the high frequency region represents the total resistance of the electrolyte, separator, and electrical contacts (R_s), whereas the semicircle in the high-frequency range indicates the charge transfer resistance (R_{ct}), which is associated with the charge transfer at the electrode–electrolyte interface. The inclined line in the low frequency region represents the Warburg impedance (Z_w), which reflects the solid-state diffusion of Li ions into the bulk of the active materials.[28,35] Comparison of these plots therefore reveals that Ge–acetylene black–Ni foam has a much lower R_{ct} than a Ge–Ni foam electrode (36.88 *vs.* 52.62 Ω). This indicates that also possesses a higher electrical conductivity, thus resulting in a better rate capability and higher reversible capacity. This can be attributed to the effective dispersion of the electrochemically active Ge nanoparticle phase in the acetylene black network, which enables efficient charge transport at the electrode–electrolyte interface. Furthermore, its 3D structure provides a large surface area, which could help relieve the volume change in the Ge nanoparticles during charge/discharge.

Conclusions

This study has demonstrated that 3D Ge–acetylene black–Ni foam composite electrodes can be easily produced by the ionic liquid electrodeposition of Ge directly onto a Ni foam that has been pre-coated in acetylene black through electrophoresis. Compared with a Ge–Ni foam electrode, the addition of acetylene black produces a satisfactory reversible discharge capacity of 924 mA h g^{-1} after 100 cycles. The excellent cycling performance and rate capability of this structure is attributed to its

electrically conductive 3D nanostructure and elastic acetylene black networks. We therefore believe that this fabrication method represents a viable and green approach for the direct assembly of nanocomposite electrodes without a binder. Moreover, such materials present a viable alternative to conventional graphite electrodes in LIBs, as they exhibit a comparable stability but higher capacity over multiple discharge/charge cycles. Indeed, their excellent high-rate capabilities suggest that 3D nano-electrodes may be suitable for high-power applications such as electric vehicles and power tools.

Acknowledgements

We thank National Natural Science Foundation of China (no. 51010005, 91216123, 51174063, 21103036), Natural Science Funds for Distinguished Young Scholar of Heilongjiang province, The Natural Science Foundation of Heilongjiang Province (E201436) and the project of International Cooperation supported by Ministry of Science and Technology of China (2013DFR10630).

Notes and references

1 B. Scrosati, *Nature*, 1995, **373**, 557–558.
2 J. M. Tarascon and M. Armand, *Nature*, 2001, **414**, 359–367.
3 P. Poizot, S. Laruelle, S. Grugeon, L. Dupont and J. M. Tarascon, *Nature*, 2000, **407**, 496–499.
4 V. Etacheri, R. Marom, R. Elazari, G. Salitra and D. Aurbach, *Energy Environ. Sci.*, 2011, **4**, 3243–3262.
5 W. Lu, A. Goering, L. T. Qu and L. M. Dai, *Phys. Chem. Chem. Phys.*, 2012, **14**, 12099–12104.
6 K. Evanoff, A. Magasinski, J. B. Yang and G. Yushin, *Adv. Energy Mater.*, 2011, **1**, 495–498.
7 Y. J. Cho, H. S. Im, H. S. Kim, Y. Myung, S. H. Back, Y. R. Lim, C. S. Jung, D. M. Jang, J. Park, E. H. Cha, W. Il Cho, F. Shojaei and H. S. Kang, *ACS Nano*, 2013, **7**, 9075–9084.
8 L. F. Cui, L. B. Hu, J. W. Choi and Y. Cui, *ACS Nano*, 2010, **4**, 3671–3678.
9 C. K. Chan, R. N. Patel, M. J. O'Connell, B. A. Korgel and Y. Cui, *ACS Nano*, 2010, **4**, 1443–1450.
10 M. H. Park, M. G. Kim, J. Joo, K. Kim, J. Kim, S. Ahn, Y. Cui and J. Cho, *Nano Lett.*, 2009, **9**, 3844–3847.
11 H. Cheng, R. Xiao, H. D. Bian, Z. Li, Y. W. Zhan, C. K. Tsang, C. Y. Chung, Z. G. Lu and Y. Y. Li, *Mater. Chem. Phys.*, 2014, **144**, 25–30.
12 M. Zhou, F. Pu, Z. Wang, T. W. Cai, H. Chen, H. Y. Zhang and S. Y. Guan, *Phys. Chem. Chem. Phys.*, 2013, **15**, 11394–11401.
13 X. Xin, X. F. Zhou, F. Wang, X. Y. Yao, X. X. Xu, Y. M. Zhu and Z. P. Liu, *J. Mater. Chem.*, 2012, **22**, 7724–7730.
14 W. H. Li, Z. Z. Yang, J. X. Cheng, X. W. Zhong, L. Gu and Y. Yu, *Nanoscale*, 2014, **6**, 4532–4537.
15 S. H. Tang, E. Y. Chang, M. Hudait, J. S. Maa, C. W. Liu, G. L. Luo, H. D. Trinh and Y. H. Su, *Appl. Phys. Lett.*, 2011, **98**, 161905-1–161905-3.
16 P. Artoni, E. F. Pecora, A. Irrera and F. Priolo, *Nanoscale Res. Lett.*, 2011, **6**, 162.
17 C. M. Hwang, C. H. Lim and J. W. Park, *Thin Solid Films*, 2011, **519**, 2332–2338.
18 A. M. Chockla, K. C. Klavetter, C. B. Mullins and B. A. Korgel, *ACS Appl. Mater. Interfaces*, 2012, **4**, 4658–4664.
19 A. Lahiri, S. Z. El Abedin and F. Endres, *J. Phys. Chem. C*, 2012, **116**, 17739–17745.
20 X. D. Meng, R. Al-Salman, J. P. Zhao, N. Borissenko, Y. Li and F. Endres, *Angew. Chem., Int. Ed.*, 2009, **48**, 2703–2707.
21 W. H. Xin, J. P. Zhao, D. T. Ge, Y. B. Ding, Y. Li and F. Endres, *Phys. Chem. Chem. Phys.*, 2013, **15**, 2421–2426.
22 X. Liu, J. P. Zhao, J. Hao, B. L. Su and Y. Li, *J. Mater. Chem. A*, 2013, **1**, 15076–15081.
23 C. K. Chan, X. F. Zhang and Y. Cui, *Nano Lett.*, 2008, **8**, 307–309.
24 G. Jo, I. Choi, H. Ahn and M. J. Park, *Chem. Commun.*, 2012, **48**, 3987–3989.
25 F. W. Yuan, H. J. Yang and H. Y. Tuan, *ACS Nano*, 2012, **6**, 9932–9942.
26 T. Kennedy, E. Mullane, H. Geaney, M. Osiak, C. O'Dwyer and K. M. Ryan, *Nano Lett.*, 2014, **14**, 716–723.
27 M. H. Park, Y. Cho, K. Kim, J. Kim, M. L. Liu and J. Cho, *Angew. Chem., Int. Ed.*, 2011, **50**, 9647–9650.
28 J. Wang, J. Z. Wang, Z. Q. Sun, X. W. Gao, C. Zhong, S. L. Chou and H. K. Liu, *J. Mater. Chem. A*, 2014, **2**, 4613–4618.
29 K. H. Seng, M. H. Park, Z. P. Guo, H. K. Liu and J. Cho, *Nano Lett.*, 2013, **13**, 1230–1236.
30 W. Li, J. Zheng, T. K. Chen, T. Wang, X. J. Wang and X. G. Li, *Chem. Commun.*, 2014, **50**, 2052–2054.
31 D. J. Xue, S. Xin, Y. Yan, K. C. Jiang, Y. X. Yin, Y. G. Guo and L. J. Wan, *J. Am. Chem. Soc.*, 2012, **134**, 2512–2515.
32 J. Liu, K. Song, C. Zhu, C.-C. Chen, P. A. van Aken, J. Maier and Y. Yu, *ACS Nano*, 2014, 7051–7059.
33 K. L. Lee, J. Y. Jung, S. W. Lee, H. S. Moon and J. W. Park, *J. Power Sources*, 2004, **129**, 270–274.
34 N. Liu, H. Wu, M. T. McDowell, Y. Yao, C. M. Wang and Y. Cui, *Nano Lett.*, 2012, **12**, 3315–3321.
35 Z. J. Zhang, J. Z. Wang, S. L. Chou, H. K. Liu, K. Ozawa and H. J. Li, *Electrochim. Acta*, 2013, **108**, 820–826.